Quantification of facial skeletal shape variation in fibroblast growth factor receptor-related craniosynostosis syndromes

Yann Heuzé, Neus Martínez-Abadías, Jennifer Stella, Eric Arnaud, Corinne Collet, Gemma García Fructuoso, Mariana Alamar, Lun-Jou Lo, Simeon Boyadjiev, Federico Di Rocco, et al.

HHS Public Access

Author manuscript

Birth Defects Res A Clin Mol Teratol. Author manuscript; available in PMC 2014 May 21.

Published in final edited form as:

Birth Defects Res A Clin Mol Teratol. 2014 April ; 100(4): 250–259. doi:10.1002/bdra.23228.

Quantification of Facial Skeletal Shape Variation in Fibroblast Growth Factor Receptor-Related Craniosynostosis Syndromes

Yann Heuzé[1], **Neus Martínez-Abadías**[1], **Jennifer M. Stella**[1], **Eric Arnaud**[2], **Corinne Collet**[3], **Gemma García Fructuoso**[4], **Mariana Alamar**[4], **Lun-Jou Lo**[5], **Simeon A. Boyadjiev**[6], **Federico Di Rocco**[2], and **Joan T. Richtsmeier**[1,*]

[1]Department of Anthropology, Pennsylvania State University, University Park, Pennsylvania

[2]Craniofacial Surgery Unit, Department of Pediatric Neurosurgery, Hôpital Necker-Enfants Malades, University Paris V, Paris, France

[3]Laboratoire de Biochimie et de Biologie Moléculaire, INSERM U606, Paris, France

[4]Servei de Neurocirurgia, Hospital Sant Joan de Deu, Barcelona, Spain

[5]Department of Plastic and Reconstructive Surgery, Chang Gung Memorial Hospital, Chang Gung University, Taoyuan, Taiwan

[6]Section of Genetics, Department of Pediatrics, University of California Davis, Sacramento, California

Abstract

Background—fibroblast growth factor receptor (FGFR) -related craniosynostosis syndromes are caused by many different mutations within FGFR-1, 2, 3, and certain FGFR mutations are associated with more than one clinical syndrome. These syndromes share coronal craniosynostosis and characteristic facial skeletal features, although Apert syndrome (AS) is characterized by a more dysmorphic facial skeleton relative to Crouzon (CS), Muenke (MS), or Pfeiffer syndromes.

Methods—Here we perform a detailed three-dimensional evaluation of facial skeletal shape in a retrospective sample of cases clinically and/or genetically diagnosed as AS, CS, MS, and Pfeiffer syndrome to quantify variation in facial dysmorphology, precisely identify specific facial features pertaining to these four syndromes, and further elucidate what knowledge of the causative FGFR mutation brings to our understanding of these syndromes.

Results—Our results confirm a strong correspondence between genotype and facial phenotype for AS and MS with severity of facial dysmorphology diminishing from Apert $FGFR2^{S252W}$ to Apert $FGFR2^{P253R}$ to MS. We show that AS facial shape variation is increased relative to CS, although CS has been shown to be caused by numerous distinct mutations within FGFRs and reduced dosage in ERF.

*Correspondence to: Joan T. Richtsmeier, Department of Anthropology, The Pennsylvania State University, Carpenter Building, University Park, PA 16802., jtr505@gmail.com.

Neus Martínez-Abadías present address is European Molecular Biology Laboratory (EMBL) - Center for Genomic Regulation (CRG) Systems Biology Research Unit, CRG, Barcelona, Spain

Conclusion—Our quantitative analysis of facial phenotypes demonstrate subtle variation within and among craniosynostosis syndromes that might, with further research, provide information about the impact of the mutation on facial skeletal and nonskeletal development. We suggest that precise studies of the phenotypic consequences of genetic mutations at many levels of analysis should accompany next-generation genetic research and that these approaches should proceed cooperatively.

Keywords

genotype-phenotype correspondence; midfacial retrusion; suture fusion; morphogenesis; diagnosis

Introduction

Cell–cell signaling through fibroblast growth factors and their receptors (FGF/FGFR) plays fundamental roles in development (Montero et al., 2000; Ornitz, 2005) and has been proposed as a key system in the evolution of the vertebrate head (Bertrand et al., 2011). The FGF/FGFR signaling system is implicated in the control of basic processes (e.g., proliferation, differentiation, migration, polarity, adhesion, apoptosis) in cells destined to become various tissues including bone and cartilage (Ornitz and Itoh, 2001; Dorey and Amaya, 2010; Li et al., 2013). Mutations in *FGFR1, 2* and *3* can lead to varied impairments of skeletal development as demonstrated by the FGFR-related craniosynostosis syndromes (i.e., Apert [AS], Beare-Stevenson, Crouzon [CS], Crouzon with acanthosis nigricans, Jackson-Weiss, Muenke [MS], and Pfeiffer [PS] syndromes). These syndromes are characterized by premature fusion of one or several cranial vault sutures associated with skull dysmorphology and potentially presenting with malformations affecting the limbs, upper airway, brain, spine, heart, and/ or lungs (Cohen and MacLean, 2000).

With the exception of MS, all FGFR-related craniosynostosis syndromes were originally defined phenotypically. Consequently, diagnosis of FGFR-related craniosynostosis syndromes is based on clinical findings (Robin et al., 1998) (e.g., craniosynostosis, dysmorphic facial features, limbs appearance) and, when possible, confirmed by genetic testing. This is important as genetic and phenotypic variation within and among craniosynostosis syndromes results in the now well-known lack of a one-toone correspondence between a given *FGFR* mutation and a specific skull shape. Some of the FGFR-related craniosynostosis syndromes can be caused by many different mutations within one or more of the *FGFR*s (e.g., PS and CS), while others are caused by a unique mutation (e.g., MS), or a very small set of mutations (e.g., AS) (Table 1). In addition, there are certain mutations in *FGFR2* that have been associated with more than one clinical syndrome (e.g., CS and PS) (Passos-Bueno et al., 2008). Consequently, in many cases clinical diagnosis is problematic.

The craniofacial phenotypes of AS, CS, MS, PS are highly variable. Craniofacial phenotypes of AS can include varying degrees of midfacial retrusion. It is reported that AS cases carrying the $FGFR2^{S252W}$ mutation have a more severe facial phenotype relative to AS patients who carry the $FGFR2^{P253R}$ mutation while the $FGFR2^{P253R}$ group has more severe limb anomalies (Slaney et al., 1996; Lajeunie et al., 1999; von Gernet et al., 2000).

Craniofacial phenotypes of CS can vary from normal, to facial skeletal dys-morphologies without calvarial craniosynostosis, to cloverleaf skull malformation. In the majority of cases, several cranial sutures are prematurely fused at birth, although on occasion, the phenotypic features of CS may be absent at birth and evolve gradually during the first few years of life (Lajeunie et al., 1999; Connolly et al., 2004; Hoefkens et al., 2004). Variation in the severity of the craniofacial phenotype and limb anomalies of PS has led to the creation of three clinical subtypes (Cohen, 1993). Finally, the craniofacial phenotype of MS is characteristically variable and ranges from normal to severe (Doherty et al., 2007).

Facial phenotype is one of the key clinical findings used in differential diagnosis among the craniosynostosis syndromes. Although AS is characterized by a more dys-morphic facial skeleton relative to CS, MS, or PS (Cohen and MacLean, 2000), all of these syndromes share characteristic facial skeletal features (i.e., Crouzonoid face), including midfacial retrusion, hypertelorism, proptosis (secondary to orbital dysmorphogenesis), high-arched palate, flattened malar region, and beaked nose (Table 1) (Robin et al., 1998; Johnson and Wilkie, 2011). Midfacial retrusion or hypoplasia is defined as the posterior positioning and/or vertical shortening of the infraorbital and perialar regions, or increased concavity of the face and/or reduced nasolabial angle representing underdevelopment of the maxillary height (decreased midface height) or depth (retrusion of the maxilla) (Allanson et al., 2009). This definition allows for a wide range of variation and currently, midfacial retrusion represents a catch-all diagnosis for many craniofacial conditions that can result from distinct molecular causes and novel developmental dynamics. Midfacial retrusion is potentially the most challenging clinical manifestation of many of the FGFR-related craniosynostosis syndromes affecting oral health, feeding, and airway function (Cunningham et al., 2007; Johnson and Wilkie, 2011) but is relatively uncommon in MS (Ridgway et al., 2011).

Here, we perform a detailed three-dimensional (3D) evaluation of facial skeletal shape in a large retrospective sample (n = 43) of cases clinically and/or genetically diagnosed as AS, CS, MS, and PS to quantify variation in severity of facial dysmorphology, and precisely identify specific facial features pertaining to one or several of these four syndromes. First, we investigate the genotype phenotype correspondence for the segment of our sample (19/43) with known genetic mutations and subsequently add the remaining cases to further elucidate what knowledge of the causative *FGFR* mutation brings to our understanding of these syndromes.

Materials and Methods

SUBJECTS

We amassed pre-operative computed tomography (CT) images of children aged 0 to 23 months acquired by several medical centers in France, United States, Taiwan, and Spain over the past 10 years. Our sample consists of images of 43 individuals genetically and/or clinically diagnosed with AS, CS, MS, or PS, and 20 unaffected individuals (Tables 2 and 3). All collected images were anonymized and no information other than sex, age at the time of the CT exam, and causative mutation were communicated to us. No data on the ethnicity or geographic origin of the patients were available. The coronal suture is prematurely fused in 38 of 43 craniosynostosis syndrome cases while three CS individuals and one AS case do

not present with craniosynostosis of any vault suture (Table 3). The causative *FGFR1–3* mutation was identified in 19 cases. Diagnosis of the remaining cases ($N = 24$) is based solely on clinical evaluation. The unaffected sample consists of images of children without craniosynostosis who underwent CT scanning for conditions not associated with craniosynostosis (e.g., seizures, suspected brain anomalies). Use of the CT images was approved by the Institutional Review Boards of the Pennsylvania State University and the participating institutions and the images were acquired in accordance with institutional guidelines.

MORPHOMETRIC DATA AND ANALYSIS

Skulls were reconstructed from the CT images using a threshold that enabled visualization of bone. A set of 39 anatomical landmarks was defined and located on the 3D reconstruction of the skull of each individual and the corresponding x, y, z coordinates were recorded with Avizo 6 (Visualization Sciences Group, SAS). In addition to the anatomical landmarks, a total of 168 semilandmarks were defined on 11 predefined curves (92 curve semiland-marks) and four surface patches (76 surface semiland-marks) on each skull (Supp. Fig. S1, which is available online; for details, see Heuzé et al., 2010 and Heuzé et al., 2012). Semilandmarks present "deficient" coordinates and were slid according to a sliding algorithm that minimizes the bending energy (Bookstein, 1997; Gunz et al., 2005) to define their final location on the defined curves or surfaces. Once slid, semilandmarks acquire a geometric correspondence across individuals so that comparative analyses can be conducted. The 3D coordinates of semilandmarks were computed using Viewbox 4 (dHAL software, Athens, Greece).

Shape information of each individual defined on the basis of landmarks and semilandmarks was extracted using general Procrustes analysis, a procedure that superimposes configurations of landmarks by shifting them to a common position, rotating and scaling them to a standard size until a best fit of corresponding landmarks is achieved (Rohlf and Slice, 1990; Dryden and Mardia, 1998). A Procrustes average shape (PAS) for a defined group was computed as the coordinate-wise average of the coordinates of the resulting centered, scaled, and rotated landmarks (Mitteroecker and Gunz, 2009). Distinct Procrustes superimpositions were used for the computation of PAS for specific skull anatomical units (Supp. Fig. S1). The PAS triangular mesh can be obtained by warping the triangular mesh of one case to the landmark set corresponding to the PAS. The covariance matrix of the Procrustes shape coordinates was analyzed by principal components analysis (PCA) (Jolliffe, 2002) to reduce the dimensionality of the dataset. PCA transforms the variables entered into the analysis into a set of new variables, the principal components (PCs), which are uncorrelated with each other. The first PC accounts for the maximum possible amount of variation and each successive PC in turn accounts for the maximum possible amount of variation that remains. Unlike discriminant analyses, PCA does not consider a priori knowledge of internal structure of the data and just rotates the data to find new axes (i.e., directions in the morphospace) that explain the maximum of morphological variation in the sample. PCA was used here to assess if the specific combination of morphological variables that explain most variation is also able to successfully separate individuals into groups of known membership (e.g., known syndrome, mutation). The PCs contain the loadings for the

linear combinations of the original variables and can be visualized as shape deformation. A simulation of a continuous shape deformation based on the available data can be obtained by warping the PAS triangular mesh along the negative (or positive) direction of each principal component. To facilitate visualization of shape differences between two PAS, we present a color map produced by comparing the corresponding surface warps. The color map has been computed in Avizo 6 (Visualization Sciences Group, VSG) and corresponds to the vector field computed by the difference of the vertex positions of corresponding vertices in both PAS surface warps.

Shape differences among groups of syndromic and unaffected individuals were estimated using Procrustes distances. The Procrustes distance is measured as the square root of the sum of squared distances between corresponding landmarks of two shape configurations after Procrustes superimposition (Dryden and Mardia, 1998; Mitteroecker and Gunz, 2009). For each comparison, the Procrustes distance between the mean shapes of the two groups considered was computed and a permutation test with 10,000 rounds was performed to test for statistical significance.

Potential influence of age on shape was explored by computing a multivariate regression of shape (Drake and Klingenberg, 2008) on age. The residuals of the multivariate regression were analyzed in a new PCA where the effect of age is removed.

Results

GENOTYPE PHENOTYPE CORRESPONDENCE FOR AS AND MS

Specifics of the mutations carried by the 19 genotyped individuals in our sample are given in Table 3 with most identified mutations associated with AS and MS. When the shape of the whole skull is analyzed using PCA of Procrustes coordinates, the first and second PCs together account for 66% of the total shape variation. Shape variation of the *FGFR2*^{S252W} AS, the *FGFR2*^{P253R} AS, and the *FGFR3*^{P250R} MS cases overlap and these groups fail to separate on the PC1 versus PC2 plot (Supp. Fig. S2A). Procrustes distances separating the mean skull shapes of the *FGFR2*^{S252W} AS group, *FGFR2*^{P253R} AS group, and *FGFR3*^{P250R} MS group are not significant (Table 4). However, when only data from the facial skeleton are analyzed by PCA, a clear separation between individuals carrying the *FGFR2*^{S252W}, *FGFR2*^{P253R}, or *FGFR3*^{P250R} mutations is revealed along PC1, which accounts for 46.9% of shape variation (Fig. 1A). The Procrustes distance separating facial shapes of the *FGFR2*^{S252W} AS group and the *FGFR3*^{P250R} MS group is significant, but the Procrustes distances between the *FGFR2*^{P253R} AS group and the *FGFR2*^{S252W} AS group and the *FGFR2*^{P253R} AS group and the *FGFR3*^{P250R} MS group are not (Table 4). The anatomical regions of the facial skeleton showing the most intense shape changes along PC1 are the frontal and zygomatic bones, the alveolar process of the maxilla and the most posterior aspect of the palate (Fig. 1B). AS cases carrying the *FGFR2*^{S252W} mutation, corresponding to the lowest scores on PC1, are characterized by increased facial width, larger orbits, posterior positioning, and vertical shortening of the maxilla and zygomatic, reduced perialar region, and a v-shaped palate with shorter length; a facial shape characteristic of midfacial retrusion. AS cases carrying the *FGFR2*^{P253R} mutation and MS cases are also located along the negative end of PC1, although not at the extreme. These groups separate from the

FGFR2^{S252W} group and from each other. According to this analysis, the *FGFR2*^{S252W} group is characterized by the most severe facial phenotype with intensity of facial dysmorphology relatively diminished in the *FGFR2*^{P253R} and *FGFR3*^{P250R} groups. These results confirm a strong correspondence between genotype and phenotype that enables differentiation of AS and MS on the basis of facial skeletal shape.

The PCA computed using the residuals of the multivariate regression of shape on age provided a very similar arrangement of the individuals indicating that the effect of age on facial and skull shape was not the main signal of the first two PCs (Supp. Figs. S2, S3).

FACIAL PHENOTYPIC VARIATION OF PATIENTS GENETICALLY AND/OR CLINICALLY DIAGNOSED WITH AS, CS, MS, OR PS

Differential diagnosis of the remaining AS, CS, and PS cases was based solely on clinical findings of craniosynostosis, specific dysmorphic facial features, and/or limb anomalies. CS and PS have been reported to display relatively similar facial phenotypes but distinct limb phenotypes. Consequently, variation of facial skeletal shape of CS and PS are expected to overlap. Although the AS facial phenotype is reported as being more severe than that of CS and PS, little quantitative information is available for comparative variation in facial shape among AS, CS, MS and PS. We quantified shape variation of the 43 individuals diagnosed genetically and/or clinically with FGFR-related craniosynostosis syndromes (Fig. 2A). The relative position of the genotyped individuals remains similar to the previous analysis that included only those patients with a genetic diagnosis (Fig. 1A), indicating that the addition of the syndromic cases that are clinically diagnosed does not change the general pattern of shape variation. Indeed, facial skeletal shape differences between the positive and negative ends of PC1 (results not shown) are the same as those reported in Figure 1B. Clinically diagnosed cases of CS occupy an intermediate position between AS and the unaffected individuals, while PS cases overlap with AS, CS, MS, and the unaffected individuals. The Procrustes distances separating the mean facial skeletal shapes of the syndromic groups are all significant with the exception of the PS-MS and PS-CS distances (Table 4). When considering the whole skull, the PC1 versus PC2 plot (59.2% of shape variation) of the skull shape analysis failed to separate the different syndromes (Supp. Fig. S5A) similar to our findings for the genotyped cases only, but the mean skull shapes of the syndromic groups displayed significant inter-group differences with the exception of the comparison of MS with AS and MS with PS (Table 4). No particular structure related to sex is observed in the PC1 versus PC2 plot of facial shape or skull shape (Supp. Figs. S4A, S5A).

The effect of age on facial and skull shape was not the main signal recorded on the corresponding PC1 versus PC2 plot as shown by the PCAs computed on the basis of the residuals of the multivariate regression of shape on age which displayed very similar arrangement of the individuals (Supp. Figs. S4, S5). To further define the anatomical location of the differences in facial shape among the FGFR-related craniosynostosis syndromes, we compared each of the syndrome specific consensus shapes (PAS) with that of all unaffected individuals (Fig. 2B). When compared with the unaffected individuals, AS and MS share similar dysmorphic features but those of MS are less severe and include some degree of asymmetry due to the presence of two MS cases with right unilateral coronal

craniosynostosis (Table 3). The anatomical regions of AS and MS displaying the most intense shape differences when compared with the unaffected individuals are the superior and inferior lateral borders of the orbits formed by the frontal and the zygomatic bones respectively, the alveolar process of the maxilla, and the most posterior aspect of the palate formed by the palatine bone. These shape differences that characterize AS and MS are very similar to those observed in Figure 1B and result in larger orbits, larger interorbital distance, reduced body and alveolar process of the maxilla, posterior positioning and vertical shortening of the infraorbital region, shorter primary palate, and shorter and superiorly projected secondary palate. The asymmetric shape differences revealed in the CS face are due to the CS cases with right unilateral coronal craniosynostosis (Table 3). Although the shape differences between CS and unaffected individuals involve the superolateral border of the orbits, the alveolar process of the maxilla, and the most posterior aspect of the palate, there is little shape difference local to the most inferior and lateral border of the orbit formed by the zygomatic bone. The shape of the nasal bridge is affected in CS but not in AS. Finally, when compared with unaffected individuals, PS displays features similar to those of CS. One key difference, however, is the reduced shape change of the alveolar process of the maxilla and the more intense shape change of the superior and lateral border of the orbit in PS relative to CS.

In summary, the nasal bridge and anterior-most aspect of the zygomatic are the anatomical regions that best differentiate AS and MS faces from those of PS and CS.

Discussion

The shape of the facial skeleton is a challenging clinical symptom and critical diagnostic feature that, along with craniosynostosis and limbs anomalies, is used to clinically diagnose FGFR-related craniosynostosis syndromes. Although based on a relatively small sample of genotyped patients (n = 19), our results reveal distinct facial phenotypes associated with $FGFR2^{S252W}$, $FGFR2^{P253R}$, and $FGFR3^{P250R}$ mutations. Such robust genotype phenotype correspondence for AS and MS does not exist when the entire skull is analyzed. Our results show a quantitative scale of severity of facial dysmorphology and particularly midfacial retrusion that is strongest in cases carrying the $FGFR2^{S252W}$ mutation, relatively decreased in the $FGFR2^{P253R}$ group and further decreased in MS. The anatomical regions displaying the most intense shape differences among AS and MS when compared with unaffected individuals are the frontal and zygomatic contributions to the orbit, and the palate. Our results are in agreement with previous studies of humans with AS and mouse models for AS in which the facial skeleton, particularly the palate, was found to be the most profoundly dysmorphic cranial feature, especially in the $FGFR2^{S252W}$ group (Slaney et al., 1996; Lajeunie et al., 1999; Von Gernet et al., 2000; Martínez-Abadías et al., 2010, 2013; Wang et al., 2010).

Three individual cases merit discussion. The CS case carrying the $FGFR2^{F276V}$ mutation displayed no sign of craniosynostosis at the age of 2 months. Because of the absence of craniosynostosis, this case plots with the unaffected cases in the skull shape analysis (Supp. Fig. S5A), while in the facial skeletal shape analysis this individual plots with the other syndromic cases (Figs. 1A, 2A). The facial phenotype and the absence of characteristic limb

anomalies prompted the diagnosis of CS for this individual, even though the *FGFR2*^{F276V} mutation has also been associated with PS (Passos-Bueno et al., 2008). These findings prompt us to propose that the *FGFR2*^{F276V} mutation functions to contribute to facial dysmorphology, perhaps by causing premature closure of facial sutures, but does not necessarily cause premature closure of the cranial vault sutures. The case carrying the *FGFR2*^{A172F} mutation that is specific to PS and known to be associated with severe limb phenotypes (Wilkie et al., 2002; Cohen, 2004), has a facial phenotype similar to that of AS (Figs. 1A, 2A). Finally, the *FGFR2*^{C342R} mutation is typically characterized by severe phenotypes (Lajeunie et al., 2006) and frequently associated with PS, although also with CS. Our case displays bilateral craniosynostosis of the coronal and lambdoid sutures and in our analysis is the second most severe facial phenotype after the PS case carrying the *FGFR2*^{F276V} mutation.

While genetic causes of CS include at least 47 distinct mutations mostly within *FGFR2* (Passos-Bueno et al., 2008), and reduced dosage of ERF (Twigg et al., 2013), the quantitative range of facial shape variation for our total CS sample is small relative to AS (Fig. 2A), which is caused by only two mutations in 99% of cases. Obviously, a small fraction of the mutations causative for CS occurs at high incidence, and only a subset of these is most likely represented in our sample. Still, we can reasonably assume that some of the cases clinically diagnosed with CS carry a different mutation than the genetically diagnosed CS case included in the present study (i.e., *FGFR2*^{F276V}). Finally, the relatively small range of MS facial shape variation revealed by our analysis contrasts with current knowledge of variation in MS with phenotypic consequences ranging from normal to severe (Doherty et al., 2007). This most likely represents an ascertainment bias in that our sample is limited to individuals who sought treatment at a medical facility and would not include individuals with normal appearance or with a mild phenotype not requiring reconstructive surgery. Consequently, our MS sample most likely represents the more severe end of the MS phenotypic continuum.

Mutations causative for FGFR-related craniosynostosis syndromes do not always determine clearly distinguishable craniofacial phenotypes and variation is substantial. Our analyses show that, even if the mean shapes of the different syndromic groups are significantly different (as measured by the inter-group Procrustes distances), the within-group variation is large, particularly for skull shape, impeding separation between groups (as shown by the PCAs of the skull shape). It is worth noting that our precise, quantitative description of the similarities and differences between the 3D facial phenotypes of AS, MS, CS, and PS leads to groupings that are similar to those obtained when groups are defined on the basis of the affected functional domain of the specific FGFR (Table 1) (Cunningham et al., 2007). Indeed, AS, MS, and FGFR1-related PS are caused by mutations within the IgII-IgIII linker region, while the majority of CS and FGFR2-dependent PS are caused by mutations within the IgIII domain. The mechanistic effect of mutations within the IgII-IgIII linker region result in altered ligand-binding specificity and/or affinity (Anderson et al., 1998; Yu et al., 2000; Ibrahimi et al., 2001, 2004), while mutations within the IgIII domain result in aberrant intermolecular disulfide bonds between unpaired cysteine residues generating constitutive activation of the receptor (Neilson and Friesel, 1996; Mangasarian et al., 1997; Robertson et

al., 1998). Although it is tempting to see a direct relationship between molecular data and our data on the corresponding craniofacial phenotypes, in the present study we identified two PS cases with facial shapes similar to AS and MS carrying *FGFR2* mutations; the $FGFR2^{A172F}$ mutation within the IgII domain and the $FGFR2^{C342R}$ mutation within the IgIII domain, instead of the anticipated *FGFR1* mutation within the IgII-IgIII linker region. Current knowledge suggests the importance of mechanisms of interaction among genes and modulation of gene expression by regulatory relationships in the making of clinical phenotypes. These dynamics, which are becoming clearer for some mutations (Sharma et al., 2013) will most likely provide the mechanistic explanation for levels of penetrance observed in patients carrying craniosynostosis mutations.

Facial reconstructive surgery, necessary in the more severe craniosynostosis cases is aimed at improving function and cosmetic appearance. Our analysis of facial skeletal dysmorphology in craniosynostosis syndromes defines distinct phenotypes and patterns of variation for diagnostic groups based on genetic and clinical information, and this should be no surprise. What our analysis brings to the field is quantitative evidence that facial dysmorphogenesis within these syndromes is not a generic event. Rather, each case of craniosynostosis results from change(s) in specific (and potentially diverse) signaling and regulatory cascades, and these changes have multiple consequences for developmental trajectories and phenotypic variation. The overall similarity in facial morphology among craniosynostosis syndromes (i.e., the Crouzonoid face) underscores the fact that generally similar phenotypes can be produced by different mutations in genes within the same or similar gene expression cascades. The differences in intensity of shared dysmorphologies observed in facial phenotypes of AS, MS, PS, and CS (Figs. 1, 2) may, with further data, provide key information about exactly which developmental pathways are being activated in a specific individual. Ideally, the synthesis of quantitative phenotypes, precise knowledge of the molecular consequences of specific mutations and their impact on developmental dynamics will reveal the mechanisms underlying craniosynostosis phenotypes providing valuable information to clinicians and surgeons managing these patients. The critical upshot would be to predict precise, individual phenotypes given genetic information (Houle, 2010).

Unraveling the complex relationship between genotype and phenotype requires levels of precision in analysis of phenotypes comparable to those used in modern genetic analysis. Our suggestion is that equally precise phenotypic analyses should accompany next-generation genetic research and that these approaches should proceed cooperatively, both in the study of animal models and humans. Not only will surgical planning be improved but new opportunities and limitations for the development of therapeutic interventions will be revealed.

Acknowledgments

This study was funded in part by the Centers for Disease Control and Prevention, the National Science Foundation, the National Institutes of Health, a Children’s Miracle Network Endowed Chair, and the American Recovery and Reinvestment Act: K23 DE00462, R03 DE016342, R01 DE016886, M01-RR00052, R01 DE018500, 3R01 DE18500-02S1, R01 DE022988; 5R01 DD000350, BCS 0725227.

We thank all study participants and their families and the following persons who participated in the CT image collection and management: Jeffrey Marsh, St. Johns Mercy HealthCare system; Jayesh Panchal, University of

Oklahoma; Alex Kane, Children's Medical Center Dallas; Benjamin Carson and Craig VanderKolk, Johns Hopkins Medical Institutions; Caroline Robson and Joan Stoler, Children's Hospital Boston; Pedro Sanchez-Lara, Children's Hospital of Los Angeles; James Boggan, University of California Davis.

References

Allanson JE, Cunniff C, Hoyme HE, et al. Elements of morphology: standard terminology for the head and face. Am J Med Genet A. 2009; 149A:6–28. [PubMed: 19125436]

Anderson J, Burns HD, Enriquez-Harris P, et al. Apert syndrome mutations in fibroblast growth factor receptor 2 exhibit increased affinity for FGF ligand. Hum Mol Genet. 1998; 7:1475–1483. [PubMed: 9700203]

Bertrand S, Camasses A, Somorjai I, et al. Amphioxus FGF signaling predicts the acquisition of vertebrate morphological traits. Proc Natl Acad Sci U S A. 2011; 108:9160–9165. [PubMed: 21571634]

Bookstein FL. Landmark methods for forms without landmarks: morphometrics of group differences in outline shape. Med Image Anal. 1997; 1:225–243. [PubMed: 9873908]

Cohen, MM. FGFs/FGFRs and association disorders. In: Epstein, CJ.; Erickson, R.; Wynshaw-Boris, A., editors. Inborn errors of development. Oxford: Oxford University Press; 2004. p. 380-400.

Cohen, MM.; MacLean, RE. Craniosynostosis: diagnosis, evaluation, and management. 2. Oxford: Oxford University Press; 2000.

Cohen MM Jr. Pfeiffer syndrome update, clinical subtypes, and guidelines for differential diagnosis. Am J Med Genet. 1993; 45:300–307. [PubMed: 8434615]

Cohen MM Jr, Kreiborg S. Birth prevalence studies of the Crouzon syndrome: comparison of direct and indirect methods. Clin Genet. 1992; 41:12–15. [PubMed: 1633640]

Cohen MM Jr, Kreiborg S, Lammer EJ, et al. Birth prevalence study of the Apert syndrome. Am J Med Genet. 1992; 42:655–659. [PubMed: 1303629]

Connolly JP, Gruss J, Seto ML, et al. Progressive postnatal craniosynostosis and increased intracranial pressure. Plast Reconstr Surg. 2004; 113:1313–1323. [PubMed: 15060342]

Cunningham ML, Seto ML, Ratisoontorn C, et al. Syndromic craniosynostosis: from history to hydrogen bonds. Orthod Craniofac Res. 2007; 10:67–81. [PubMed: 17552943]

Doherty ES, Lacbawan F, Hadley DW, et al. Muenke syndrome (FGFR3-related craniosynostosis): expansion of the phenotype and review of the literature. Am J Med Genet A. 2007; 143A:3204–3215. [PubMed: 18000976]

Dorey K, Amaya E. FGF signalling: diverse roles during early vertebrate embryogenesis. Development. 2010; 137:3731–3742. [PubMed: 20978071]

Drake AG, Klingenberg CP. The pace of morphological change: historical transformation of skull shape in St Bernard dogs. Proc Biol Sci. 2008; 275:71–76. [PubMed: 17956847]

Dryden, IL.; Mardia, KV. Statistical shape analysis. Chichester: Wiley; 1998.

Gunz, P.; Mitteroecker, P.; Bookstein, FL. Semilandmarks in three dimensions. In: Slice, DE., editor. Modern morphometrics in physical anthropology. New York: Kluwer Academic/Plenum Publishers; 2005. p. 73-98.

Heuzé Y, Boyadjiev SA, Marsh JLK, et al. New insights into the relationship between suture closure and craniofacial dysmorphology in sagittal nonsyndromic craniosynostosis. J Anat. 2010; 217:85–96. [PubMed: 20572900]

Heuzé Y, Martínez-Abadías N, Stella JM, et al. Unilateral and bilateral expression of a quantitative trait: asymmetry and symmetry in coronal craniosynostosis. J Exp Zoolog B Mol Dev Evol. 2012; 318:109–122.

Hoefkens MF, Vermeij-Keers C, Vaandrager JM. Crouzon syndrome: phenotypic signs and symptoms of the postnatally expressed subtype. J Craniofac Surg. 2004; 15:233–240. discussion 241–242. [PubMed: 15167238]

Houle D. Numbering the hairs on our heads: the shared challenge and promise of phenomics. Proc Natl Acad Sci U S A. 2010; 107(Suppl 1):1793–1799. [PubMed: 19858477]

Ibrahimi OA, Eliseenkova AV, Plotnikov AN, et al. Structural basis for fibroblast growth factor receptor 2 activation in Apert syndrome. Proc Natl Acad Sci U S A. 2001; 98:7182–7187. [PubMed: 11390973]

Ibrahimi OA, Zhang F, Eliseenkova AV, et al. Biochemical analysis of pathogenic ligand-dependent FGFR2 mutations suggests distinct pathophysiological mechanisms for craniofacial and limb abnormalities. Hum Mol Genet. 2004; 13:2313–2324. [PubMed: 15282208]

Johnson D, Wilkie AOM. Craniosynostosis. Eur J Hum Genet. 2011; 19:369–376. [PubMed: 21248745]

Jolliffe, IT. Principal component analysis. New York: Springer; 2002.

Lajeunie E, Cameron R, El Ghouzzi V, et al. Clinical variability in patients with Apert's syndrome. J Neurosurg. 1999; 90:443–447. [PubMed: 10067911]

Lajeunie E, Heuertz S, El Ghouzzi V, et al. Mutation screening in patients with syndromic craniosynostoses indicates that a limited number of recurrent FGFR2 mutations accounts for severe forms of Pfeiffer syndrome. Eur J Hum Genet. 2006; 14:289–298. [PubMed: 16418739]

Li X, Young NM, Tropp S, et al. Quantification of shape and cell polarity reveals a novel mechanism underlying malformations resulting from related FGF mutations during facial morphogenesis. Hum Mol Genet. 2013; 22:5160–5172. [PubMed: 23906837]

Mangasarian K, Li Y, Mansukhani A, Basilico C. Mutation associated with Crouzon syndrome causes ligand-independent dimerization and activation of FGF receptor-2. J Cell Physiol. 1997; 172:117–125. [PubMed: 9207932]

Martínez-Abadías N, Holmes G, Pankratz T, et al. From shape to cells: mouse models reveal mechanisms altering palate development in Apert syndrome. Dis Model Mech. 2013; 6:768–779. [PubMed: 23519026]

Martínez-Abadías N, Percival C, Aldridge K, et al. Beyond the closed suture in apert syndrome mouse models: evidence of primary effects of FGFR2 signaling on facial shape at birth. Dev Dyn. 2010; 239:3058–3071. [PubMed: 20842696]

Mitteroecker P, Gunz P. Advances in geometric morphometrics. Evol Biol. 2009; 36:235–247.

Montero A, Okada Y, Tomita M, et al. Disruption of the fibroblast growth factor-2 gene results in decreased bone mass and bone formation. J Clin Invest. 2000; 105:1085–1093. [PubMed: 10772653]

Neilson KM, Friesel R. Ligand-independent activation of fibroblast growth factor receptors by point mutations in the extracellular, transmembrane, and kinase domains. J Biol Chem. 1996; 271:25049–25057. [PubMed: 8798788]

Oldridge M, Zackai EH, McDonald-McGinn DM, et al. De novo alu-element insertions in FGFR2 identify a distinct pathological basis for Apert syndrome. Am J Hum Genet. 1999; 64:446–461. [PubMed: 9973282]

Ornitz DM. FGF signaling in the developing endochondral skeleton. Cytokine Growth Factor Rev. 2005; 16:205–213. [PubMed: 15863035]

Ornitz DM, Itoh N. Fibroblast growth factors. Genome Biol. 2001; 2:REVIEWS3005. [PubMed: 11276432]

Passos-Bueno MR, Serti Eacute AE, Jehee FS, et al. Genetics of craniosynostosis: genes, syndromes, mutations and genotype-phenotype correlations. Front Oral Biol. 2008; 12:107–143. [PubMed: 18391498]

Ridgway EB, Wu JK, Sullivan SR, et al. Craniofacial growth in patients with FGFR3Pro250Arg mutation after fronto-orbital advancement in infancy. J Craniofac Surg. 2011; 22:455–461. [PubMed: 21403567]

Robertson SC, Meyer AN, Hart KC, et al. Activating mutations in the extracellular domain of the fibroblast growth factor receptor 2 function by disruption of the disulfide bond in the third immunoglobulin-like domain. Proc Natl Acad Sci U S A. 1998; 95:4567–4572. [PubMed: 9539778]

Robin, NH.; Falk, MJ.; Haldeman-Englert, CR. GeneReviews™ [Internet]. In: Pagon, RA.; Adam, MP.; Bird, TD.; Dolan, CR.; Fong, CT.; Stephens, K., editors. FGFR-related craniosynostosis syndromes. Seattle: University of Washington; 1998–2011. Available at: http://www.ncbi.nlm.nih.gov/books/NBK1455 [Accessed December 17, 2012]

Rohlf F, Slice D. Extensions of the Procrustes method for the optimal superimposition of landmarks. Syst Zool. 1990; 39:40–59.

Sharma VP, Fenwick AL, Brockop MS, et al. Mutations in TCF12, encoding a basic helix-loop-helix partner of TWIST1, are a frequent cause of coronal craniosynostosis. Nat Genet. 2013; 45:304–307. [PubMed: 23354436]

Slaney SF, Oldridge M, Hurst JA, et al. Differential effects of FGFR2 mutations on syndactyly and cleft palate in Apert syndrome. Am J Hum Genet. 1996; 58:923–932. [PubMed: 8651276]

Twigg SRF, Vorgia E, McGowan SJ, et al. Reduced dosage of ERF causes complex craniosynostosis in humans and mice and links ERK1/2 signaling to regulation of osteogenesis. Nat Genet. 2013; 45:308–313. [PubMed: 23354439]

Vogels A, Fryns J-P. Pfeiffer syndrome. Orphanet J Rare Dis. 2006; 1:19. [PubMed: 16740155]

Von Gernet S, Golla A, Ehrenfels Y, et al. Genotype-phenotype analysis in Apert syndrome suggests opposite effects of the two recurrent mutations on syndactyly and outcome of craniofacial surgery. Clin Genet. 2000; 57:137–139. [PubMed: 10735635]

Wang Y, Sun M, Uhlhorn VL, et al. Activation of p38 MAPK pathway in the skull abnormalities of Apert syndrome Fgfr2(+P253R) mice. BMC Dev Biol. 2010; 10:22. [PubMed: 20175913]

Wilkie AOM. Bad bones, absent smell, selfish testes: the pleiotropic consequences of human FGF receptor mutations. Cytokine Growth Factor Rev. 2005; 16:187–203. [PubMed: 15863034]

Wilkie AOM, Byren JC, Hurst JA, et al. Prevalence and complications of single-gene and chromosomal disorders in craniosynostosis. Pediatrics. 2010; 126:e391–e400. [PubMed: 20643727]

Wilkie AOM, Patey SJ, Kan S-H, et al. FGFs, their receptors, and human limb malformations: clinical and molecular correlations. Am J Med Genet. 2002; 112:266–278. [PubMed: 12357470]

Yu K, Herr AB, Waksman G, Ornitz DM. Loss of fibroblast growth factor receptor 2 ligand-binding specificity in Apert syndrome. Proc Natl Acad Sci U S A. 2000; 97:14536–14541. [PubMed: 11121055]

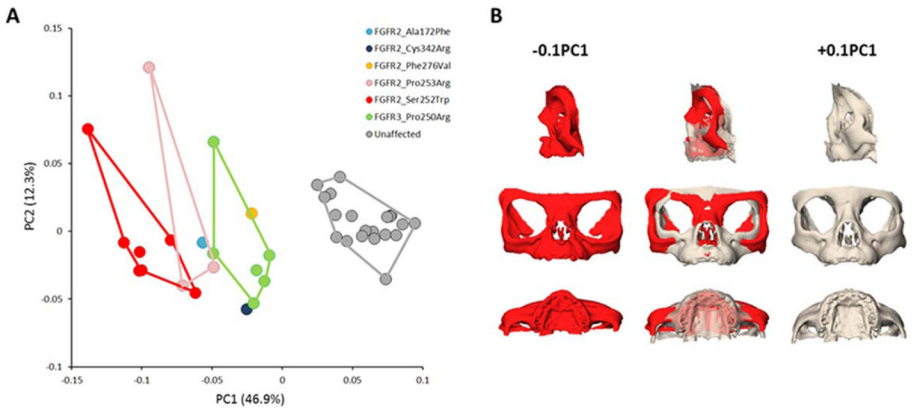

FIGURE 1.

Genotype phenotype correspondence in FGFR-related craniosynostosis syndromes. **A:** Placement of the syndromic cases and unaffected individuals on PC1 and PC2 in the shape space (principal components analysis of the Procrustes shape coordinates) when analyzing all landmarks and semilandmarks measured on the facial skeleton. **B:** Shape changes associated with PC1 when analyzing the facial skeleton. The warped facial skeleton in red corresponds to the facial shape of the *FGFR2*^{S252W} group while the warped facial skeleton in gray corresponds to the facial shape of the unaffected individuals.

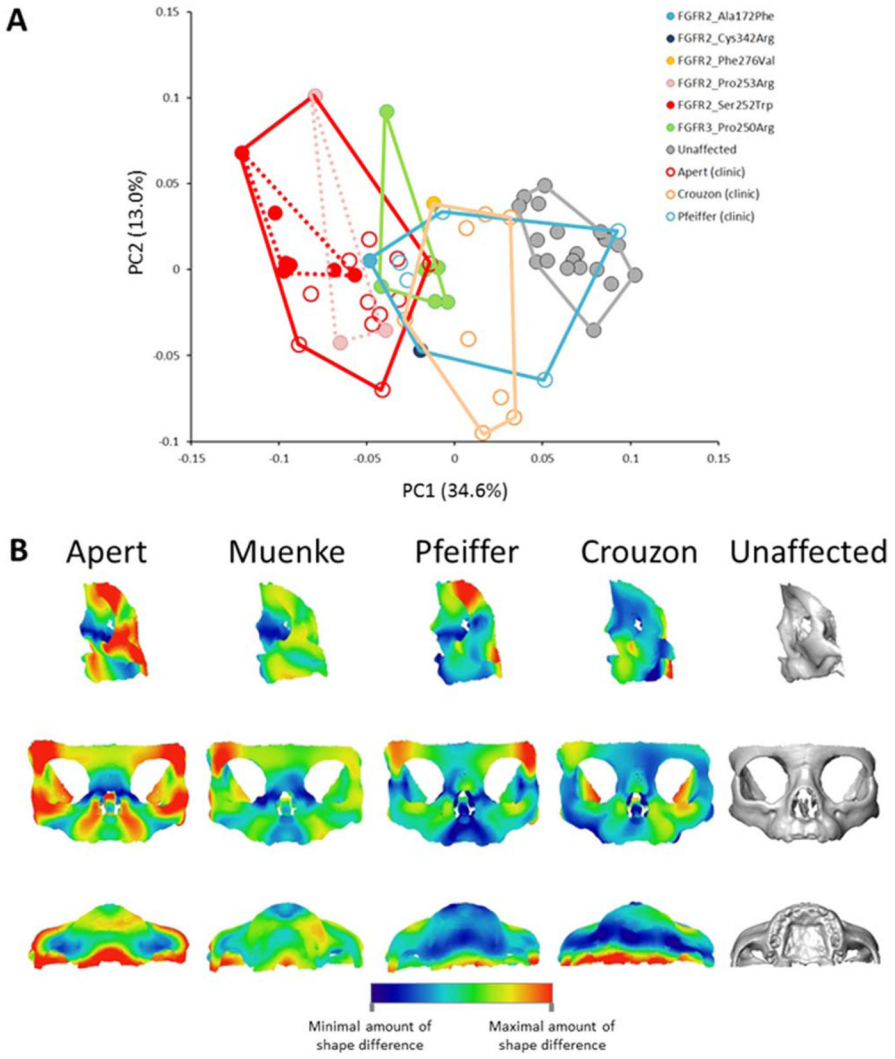

FIGURE 2.

Facial phenotypic variation of patients genetically and/or clinically diagnosed with AS, CS, MS, or PS. **A:** Placement of the syndromic cases and unaffected individuals on PC1 and PC2 in the shape space (principal components analysis of the Procrustes shape coordinates) when analyzing all landmarks and semilandmarks measured on the facial skeleton. *Filled circles*: patients genetically diagnosed; *open circles*: patients clinically diagnosed. **B:** Lateral, anterior and inferior views of the mean shape differences between the facial skeleton of AS, MS, PS, CS and unaffected individuals. Colors represent the magnitude of shape differences between the consensus shape (PAS) of each syndrome (AS, MS, PS, or CS) and the unaffected PAS computed as the difference of the vertex positions of corresponding vertices in both triangular meshes.

TABLE 1

Molecular and Phenotypic Information Pertaining to Apert, Crouzon, Muenke, and Pfeiffer Syndromes.

Genes Involved (no. of Known Mutations)	Syndrome	Birth Prevalence per 1,000,000 births	Clinical Craniofacial Phenotypes	Clinical Limbs Phenotypes	FGFR Functional Domain
FGFR1(1)	Pfeiffer	0.5 (Robin et al., 1998; Vogels and Fryns, 2006)	Craniosynostosis, midfacial hypoplasia, ocular proptosis, hypertelorism	Broad first digits, brachydactyly, variable syndactyly	IgII-IgIII linker region
FGFR2 (2[a])	Apert	10–15.5 (Cohen et al., 1992; Robin et al., 1998)	Coronal craniosynostosis, midfacial hypoplasia, sagittal and metopic sutural agenesis, acrobrachycephaly, ocular proptosis, hypertelorism, highly arched and constricted palate	Hands and feet syndactyly	IgII-IgIII linker region
FGFR2 (40)	Crouzon	15 (Cohen and Kreiborg, 1992)	Craniosynostosis midfacial hypoplasia, ocular proptosis, hypertelorism, arched palate	Normal	IgIII domain[b]
FGFR2 (29)	Pfeiffer	9 (Robin et al., 1998; Vogels and Fryns, 2006)	More severe craniosynostosis, ocular propotosis and midfacial hypoplasia than FGFR1-related Pfeiffer, hypertelorism	Broader thumbs than FGFR1-related Pfeiffer, broad toes, brachydactyly, variable syndactyly	IgIII domain[b]
FGFR3 (1)	Muenke	33.5 (Wilkie et al., 2010)	Coronal craniosynostosis, highly arched palate, variable facial dymorphisms	Variable carpal and tarsal fusion, variable broad great toes	IgII-IgIII linker region

[a] Apert syndrome can be rarely caused by Alu insertion (Oldridge et al., 1999).

[b] About 15% of *FGFR2* mutations associated with Pfeiffer or Crouzon syndromes have been identified within IgII, IgII-IgIII linker region, and the tyrosine kinase domain (Wilkie, 2005; Passos-Bueno et al., 2008).

Birth Defects Res A Clin Mol Teratol. Author manuscript; available in PMC 2014 May 21.

TABLE 2

Distribution of the Type of Data by Medical Center.

	CT Images		DNA	
	SC	Unaffected	SC	Unaffected
Hôpital Necker Enfants Malades, Paris, France	15	0	15	0
Chang Gung Memorial Hospital, Taiwan	9	0	0	0
Children's Hospital Saint Louis, Washington University, MO	6	9	0	0
Johns Hopkins Hospital, Baltimore, MD	3	3	1	0
Children's Hospital of Los Angeles, CA	3	0	1	0
Hospital Sant Joan de Deu, Barcelona, Spain	3	0	0	0
Children's Hospital Oklahoma, Oklahoma University, OK	2	8	0	0
The Children's Medical Center, Dayton, OH	1	0	1	0
Mercy General Medical Center, Sacramento, CA	1	0	1	0
Boston Children's Hospital, MA	0	0	0	0
University of California Davis, Sacramento, CA	0	0	0	0
Total	43	20	19	0

CT, computed images; SC, syndromic craniosynostosis.

TABLE 3

Distribution of Age, Sex, Type of Craniosynostosis and Identified Mutations by Phenotype.

	N (F;M)	Mean Age in Months (SD)	Type of Craniosynostosis (N)	Genetic Data (N)
Apert	21 (11;10)	6.3 (6.6)	BCS (16); BCS+LULS (2); BCS+RULS (1); RUCS (1); None (1)	$FGFR2^{S252W}$ (7); $FGFR2^{P253R}$ (3)
Crouzon	9 (3;6)	6.0 (3.3)	BCS (1); BCS+BLS+SS (1); BLS (1); RUCS (2); RUCS+BLS +SS (1); None (3)	$FGFR2^{F276V}$ (1)
Pfeiffer	7 (5;2)	7.3 (7.9)	BCS (2); BCS+BLS (1); BCS+SS (1); LUCS (2); LUCS+SS (1)	$FGFR2^{A172F}$ (1); $FGFR2^{C342R}$ (1)
Muenke	6 (3;3)	4.8 (2.6)	BCS (3); BCS+LULS (1); RUCS (2)	$FGFR3^{P250R}$ (6)
Unaffected	20 (10;10)	10.7 (6.8)	None (20)	

BCS, bicoronal synostosis; BLS, bilambdoid synostosis; SS, sagittal synostosis; RUCS, right unicoronal synostosis; LUCS, left unicoronal synostosis; LULS, left unilambdoid synostosis; None, no sign of craniosynostosis.

TABLE 4

Procrustes Distances between Groups and Corresponding *p*-Values after Permutation Test with 10,000 Rounds.

Faces of the genotyped cases				
	$FGFR2^{P253R}$	$FGFR2^{S252W}$	$FGFR3^{P250R}$	
$FGFR2^{S252W}$	0.074 (0.1564)			
$FGFR3^{P250R}$	0.0915 (0.1169)	0.0866 (0.0033)		
None	0.1414 (0.0004)	0.1601 (<0.0001)	0.0964 (<0.0001)	
Skulls of the genotyped cases				
	$FGFR2^{P253R}$	$FGFR2^{S252W}$	$FGFR3^{P250R}$	
$FGFR2^{S252W}$	0.0531 (0.407)			
$FGFR3^{P250R}$	0.06 (0.379)	0.0598 (0.0872)		
None	0.1462 (0.0001)	0.1491 (<0.0001)	0.1225 (<0.0001)	
Faces of the genotyped and clinically diagnosed cases				
	Apert	Crouzon	Muenke	Pfeiffer
Crouzon	0.0908 (<0.0001)			
Muenke	0.0661 (0.0104)	0.0788 (0.004)		
Pfeiffer	0.0774 (0.0011)	0.0612 (0.0863)	0.0661 (0.1254)	
Unaffected	0.1339 (<0.0001)	0.0795 (<0.0001)	0.0963 (<0.0001)	0.0829 (<0.0001)
Skulls of the genotyped and clinically diagnosed cases				
	Apert	Crouzon	Muenke	Pfeiffer
Crouzon	0.105 (<.0001)			
Muenke	0.0484 (0.0951)	0.095 (0.0001)		
Pfeiffer	0.0681 (0.003)	0.0647 (0.0082)	0.0672 (0.0713)	
Unaffected	0.1459 (<0.0001)	0.0888 (<0.0001)	0.1225 (<0.0001)	0.1016 (<0.0001)